

# On the Color Dipole Picture <sup>1</sup>

Dieter Schildknecht<sup>1,2,a)</sup>

<sup>1</sup>Universität Bielefeld, Fakultät für Physik Universitätsstraße 25, D-33615 Bielefeld

<sup>2</sup>Max-Planck-Institut für Physik Föhringer Ring 6, D-80805 München

<sup>a)</sup>Corresponding author: schild@physik.uni-bielefeld.de

URL: <http://www.physik.uni-bielefeld.de>

**Abstract.** We give a brief representation of the theoretical results from the color dipole picture, covering the total photoabsorption cross section, high-energy  $J/\psi$  photoproduction with respect to recent experimental data from the LHCb Collaboration at CERN, and ultra-high energy neutrino scattering, relevant for the ICE-CUBE experiment.

## DEEP INELASTIC SCATTERING

In terms of the imaginary part of the (virtual) forward Compton-scattering amplitude, deep inelastic electron-proton scattering at low values of  $x \cong Q^2/W^2 \lesssim 0.1$  proceeds via  $q\bar{q}$  forward scattering, compare Figure 1.

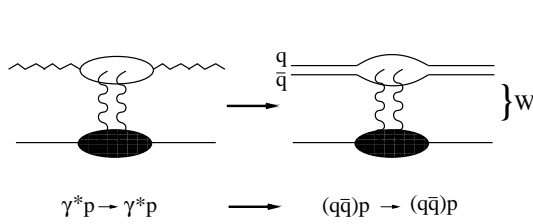


Figure 1: Relation between  $\gamma^*p \rightarrow \gamma^*p$  and  $(q\bar{q})p \rightarrow (q\bar{q})p$

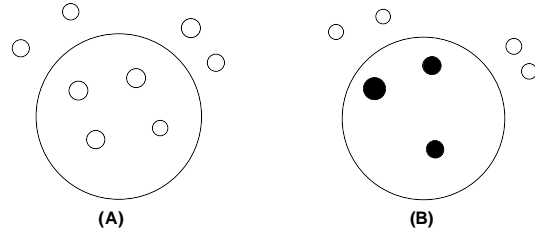


Figure 2: Color Transparency (A) and Saturation (B)

The total photoabsorption cross section is determined by (color-dipole picture, CDP)

$$\sigma_{\gamma_{T,L}^*p}(W^2, Q^2) = \int dz \int d^2r_{\perp} |\psi_{T,L}(r_{\perp}, z(1-z), Q^2)|^2 \sigma_{(q\bar{q})_{T,L}^*p}(\vec{r}_{\perp} \sqrt{z(1-z)}, W^2). \quad (1)$$

Compare e.g. refs. [1] for a presentation of the CDP and a list of literature. In standard notation,  $|\psi_{T,L}(r_{\perp}, z(1-z), Q^2)|^2$  denotes the probability for the photon of virtuality  $Q^2$  to couple to a  $(q\bar{q})_{T,L}^*$  state specified by the transverse size  $\vec{r}_{\perp}$  and the longitudinal momentum partition  $0 \leq z \leq 1$ , and  $\sigma_{(q\bar{q})_{T,L}^*p}(\vec{r}_{\perp} \sqrt{z(1-z)}, W^2)$  denotes the color-dipole-proton cross section at the total  $\gamma^*p$  center-of-mass energy  $W$ . The gauge-invariant two-gluon coupling of the  $q\bar{q}$  dipole in Figure 1 requires a representation of the  $(q\bar{q})$ -color-dipole-proton cross section of the form

$$\sigma_{(q\bar{q})_{T,L}^*p}(\vec{r}_{\perp} \sqrt{z(1-z)}, W^2) = \int d^2l'_{\perp} \bar{\sigma}_{(q\bar{q})_{T,L}^*p}(\vec{l}'_{\perp}, W^2) (1 - e^{-\vec{l}'_{\perp} \cdot \vec{r}_{\perp} \sqrt{z(1-z)}}). \quad (2)$$

Note the factorization in (1) into the  $Q^2$ -dependent “photon wave function”, and the  $W^2$ -dependence  $(q\bar{q})p$  cross section. The photon wave function is known from quantum electrodynamics. It implies that at sufficiently large values of  $Q^2$  only small dipoles of transverse size  $\vec{r}_{\perp}^2 \sim 1/Q^2$  contribute to the interaction.

Concerning the  $\vec{r}_{\perp}^2$  dependence of the dipole cross section in (2), with an energy-dependent upper limit,  $\vec{l}'_{\perp} \leq \vec{l}'_{\perp Max}(W^2)$  in (2), for any fixed dipole size  $\vec{r}_{\perp}^2$ , we either have i)  $\vec{l}'_{\perp Max}(W^2) \vec{r}_{\perp}^2 \ll 1$ , implying  $\sigma_{(q\bar{q})p} \sim \vec{r}_{\perp}^2$ , (“color transparency”), or ii)  $\vec{l}'_{\perp Max}(W^2) \vec{r}_{\perp}^2 \gg 1$ , implying  $\sigma_{(q\bar{q})p} \sim \sigma^{(\infty)}(W^2)$ , (“saturation”), compare Figure 2.

Evaluation of the photoabsorption cross section (1), upon inserting the dipole cross section in the limits i) and ii), translates color transparency (c.tr.) and saturation (sat.) into specified limits of photoabsorption [1, 2].

$$\sigma_{\gamma^*p}(W^2, Q^2) = \sigma_{\gamma^*p}(\eta(W^2, Q^2)) \sim \sigma^{(\infty)}(W^2) \begin{cases} \frac{1}{\eta(W^2, Q^2)} & , \quad \text{for } \eta(W^2, Q^2) \gg 1, \text{ c.tr.} \\ \ln \frac{1}{\eta(W^2, Q^2)} & , \quad \text{for } \eta(W^2, Q^2) \ll 1, \text{ sat.} \end{cases} \quad (3)$$

<sup>1</sup>Presented at Diffraction 2016, Acireale (Catania, Sicily) September 2-8, 2016, AIP Conference Proceedings, ed. by A. Papa, to be published

With  $\sigma^{(\infty)}(W^2) \approx \text{const}$ , the photoabsorption cross section only depends on the single low- $x$  scaling variable  $\eta(W^2, Q^2) = (Q^2 + m_0^2)/(\Lambda_{sat}^2(W^2))$ . The ‘‘saturation scale’’,  $\Lambda_{sat}^2(W^2)$  is determined by the first moment of  $\bar{\sigma}_{(q\bar{q})_{T,L}^{J=1}P}(\vec{l}'^2, W^2)$  in (2), and  $m_0^2 \lesssim m_p^2$  for light quarks is fixed by quark-hadron duality. Actually,  $\sigma^{(\infty)} \sim \ln W^2$ , i.e. logarithmic violation of  $\eta$ -scaling.

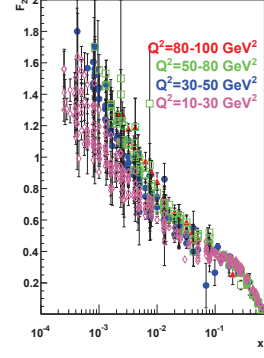
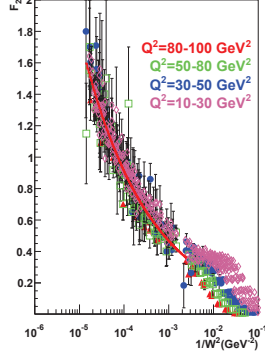
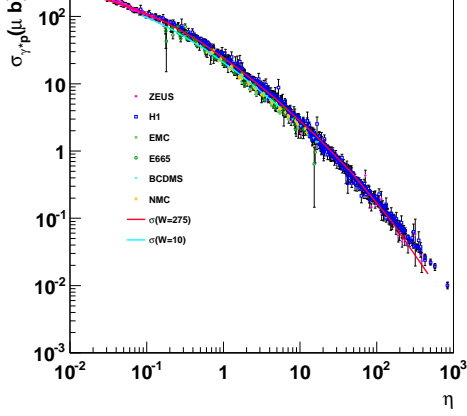


Figure 3:  $\sigma_{\gamma^*p}(W^2, Q^2) = \sigma_{\gamma^*p}(\eta(W^2, Q^2))$ .

Figure 4: Proton structure function  $F_2(x, Q^2)$ .

We summarize: the gauge-invariant two-gluon coupling of the color dipole implies color transparency and saturation, which translate into  $\sigma_{\gamma^*p} \sim 1/\eta(W^2, Q^2)$  and  $\sigma_{\gamma^*p} \sim \ln(1/\eta(W^2, Q^2))$ , respectively. No specific free-parameter-dependent ansatz is necessary to arrive at this conclusion. The experimental results agree with the above prediction, compare Figure 3. From (3), for  $W^2 \rightarrow \infty$  with  $Q^2 > 0$  fixed,  $\sigma_{\gamma^*p}(\eta(W^2, Q^2))$  approaches [2] the  $Q^2 = 0$  photoproduction limit. Compare Ref. [1] for results on the longitudinal-to-transverse ratio. In Figure 4, we show the proton structure function. In the color-transparency region, as a consequence from  $\sigma_{\gamma^*p} \sim 1/\eta(W^2, Q^2)$ , we have  $F_2(x, Q^2) = F_2(W^2)$ .

### PHOTOPRODUCTION AND ELECTROPRODUCTION OF THE $J/\psi$ VECTOR MESON

As depicted in Figure 5, the diffractive production of  $q\bar{q}$  pairs, in distinction from the total photoabsorption cross section in (1), depends on the square of the  $(q\bar{q})$ -proton cross section. Employing quark-hadron duality, diffractive vector-meson production is obtained by integration of  $q\bar{q}$  production over the mass interval that it determined by the level spacing of the vector meson states under consideration. In view of recent  $J/\psi$ -

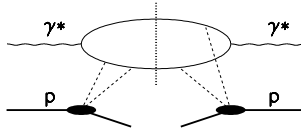


Figure 5: Diffractive  $q\bar{q}$ -pair production

photoproduction data [3] from the LHCb collaboration, we concentrate [4] on  $J/\psi$  production. Approximating  $(c\bar{c})$ -production by the cross section at the production threshold simplifies the integration over the level spacing  $\Delta M_{J/\psi}^2$ . This integration yields a factor  $\Delta F^2(m_c^2, \Delta M_{J/\psi}^2)$ , compare details in ref. [5]. Upon suppressing an overall constant factor, the  $Q^2$  dependence and the  $W^2$  dependence are given by [4]

$$\left. \frac{d\sigma_{\gamma^*p \rightarrow J/\psi p}(W^2, Q^2)}{dt} \right|_{t \approx 0} \propto \frac{(\sigma^{(\infty)}(W^2))^2}{\left(1 + \frac{Q^2 + M_{J/\psi}^2}{\Lambda_{sat}^2(W^2)}\right)^2} \frac{\Delta F^2(m_c^2, \Delta M_{J/\psi}^2)}{(Q^2 + M_{J/\psi}^2)} \cong \begin{cases} \frac{\Lambda_{sat}^4(W^2)(\sigma^{(\infty)}(W^2))^2}{(Q^2 + M_{J/\psi}^2)^2} \frac{\Delta F^2(m_c^2, \Delta M_{J/\psi}^2)}{(Q^2 + M_{J/\psi}^2)} \\ (\sigma^{(\infty)}(W^2))^2 \frac{\Delta F^2(m_c^2, \Delta M_{J/\psi}^2)}{(Q^2 + M_{J/\psi}^2)} \end{cases} \quad (4)$$

where the first line on the right-hand side refers to  $\eta_{c\bar{c}}(W^2, Q^2) \equiv (Q^2 + M_{J/\psi}^2)/\Lambda_{sat}^2(W^2) \gg 1$ , while the second line refers to  $\eta_{c\bar{c}}(W^2, Q^2) \equiv (Q^2 + M_{J/\psi}^2)/\Lambda_{sat}^2(W^2) \ll 1$ .

At any fixed value of  $Q^2$ , for the  $W$ -dependence in (4), we have the significant limits of  $\eta_{c\bar{c}}(W^2, Q^2) \gg 1$  and  $\eta_{c\bar{c}}(W^2, Q^2) \ll 1$ , where  $\eta_{c\bar{c}}(W^2, Q^2)$  generalizes the low- $x$  scaling variable  $\eta(W^2, Q^2)$ . The limits in (4), respectively, correspond to color transparency and saturation for  $J/\psi$  production. Note that (4) yields a

parameter-free prediction for  $J/\psi$  production, once  $\sigma^{(\infty)}(W^2)$  and  $\Lambda_{sat}^2(W^2)$  are known from the measurements of the total photoabsorption cross section (1).

For the comparison of the  $Q^2$  dependence and the  $W^2$  dependence in (4) with the experimental data in the HERA energy range of  $W \lesssim 300$  GeV, we refer to ref. [5]. The figures in ref. [5] show good agreement of the prediction (4) with the experimental data.

Turning to photoproduction at  $W \gtrsim 100$  GeV, from (4), we obtain

$$\begin{aligned} \sigma_{\gamma p \rightarrow J/\psi p}(W^2) &= \frac{\left(1 + \frac{M_{J/\psi}^2}{\Lambda_{sat}^2(W_1^2)}\right)^2}{\left(1 + \frac{M_{J/\psi}^2}{\Lambda_{sat}^2(W^2)}\right)^2} \frac{(\sigma^{(\infty)}(W^2))^2}{(\sigma^{(\infty)}(W_1^2))^2} \sigma_{\gamma p \rightarrow J/\psi p}(W_1^2 = (100 \text{ GeV})^2), \\ &\equiv F_A(\Lambda_{sat}^2(W^2)) F_B(W^2) \sigma_{\gamma p \rightarrow J/\psi p}(W_1^2 = (100 \text{ GeV})^2), \end{aligned} \quad (5)$$

where  $\sigma_{\gamma p \rightarrow J/\psi p}(W_1^2 = (100 \text{ GeV})^2) = 80 \text{ nb}$  is to be inserted on the right-hand side. From (5), one finds the numerical results [4] given in the last column of Table 1.

Table 1: The  $W$ -dependence of  $J/\psi$  photoproduction.

$W$ [GeV]	$\Lambda_{sat}^2(W^2)$ [GeV <sup>2</sup> ]	$\frac{M_{J/\psi}^2}{\Lambda_{sat}^2(W^2)}$	$F_A(\Lambda_{sat}^2(W^2))$	$F_B(W^2)$	$\sigma_{\gamma p \rightarrow J/\psi p}(W)$ [nb]
100	4.32	2.22	1	1	80
300	7.92	1.21	2.12	1.02	173
1000	15.4	0.624	3.93	1.11	349
2000	22.6	0.425	5.11	1.16	474

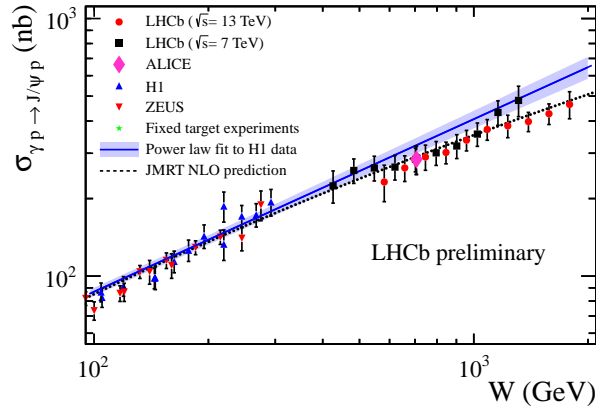


Figure 6: The LHCb data (from ref. [3])

Comparison with the experimental data in Figure 6, taken from ref. [3], shows agreement with our predictions in the last column of Table 1. According to Table 1, the experimental data from the LHCb collaboration, with  $\eta_{c\bar{c}}(W^2, Q^2 = 0) = M_{J/\psi}^2/\Lambda_{sat}^2(W^2)$ , lie in the range of  $2.2 \gtrsim \eta_{c\bar{c}}(W^2, Q^2) \gtrsim 0.43$ . This region of  $\eta_{c\bar{c}}$ , according to (4), covers the transition from color transparency to saturation; the deviation from the power-law fit in Figure 6 is to be interpreted as a transition from color transparency to saturation. We stress that the frequently assumed proportionality of  $J/\psi$  photoproduction to the square of the gluon distribution, corresponding to  $\Lambda_{sat}^4(W^2) \sim (\alpha_s(Q^2)xg(x, Q^2))^2$ , violates the necessary decent (logarithmic) high-energy saturation behavior that is naturally contained in our prediction from the CDP.

## THE NEUTRINO-NUCLEON CROSS SECTION AT ULTRA-HIGH ENERGIES

Predictions of the neutrino-nucleon cross section at ultrahigh energies of the order of  $E = 10^6$  GeV and beyond are relevant and important for the interpretation of the search for cosmic neutrinos in e.g. the ICE-CUBE experiment. Due to the presence of the  $W$ -boson mass in conjunction with ultrahigh energy, the process is determined by  $x \simeq Q^2/W^2 \ll 0.1$ . For the flavor-independent interaction of  $q\bar{q}$  pairs, the neutrino cross

section is related to  $\sigma_{\gamma^*p}(\eta(W^2, Q^2))$  by [6]

$$\sigma_{\nu N}(E) = \frac{G_F^2 M_W^4}{8\pi^3 \alpha} \frac{n_f}{\sum_q Q_q^2} \int_{Q_{Min}^2}^{s-M_p^2} dQ^2 \frac{Q^2}{(Q^2 + M_W^2)^2} \int_{M_p^2}^{s-Q^2} \frac{dW^2}{W^2} \frac{1}{2} (1 + (1-y)^2) \sigma_{\gamma^*p}(\eta(W^2, Q^2)). \quad (6)$$

where  $n_f/\sum_q Q_q^2 = 5/18$  for  $n_f = 4$  quark flavors. A careful evaluation of the cross section shows that the cross section, even at energies of the order of  $E \sim 10^{10}$  GeV is dominated by the color-transparency region, where  $\sigma_{\gamma^*p} \sim 1/\eta(W^2, Q^2)$ .

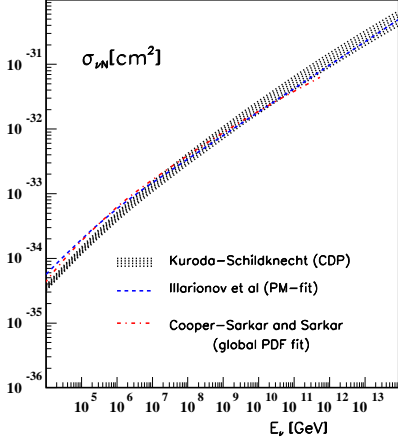


Figure 7: The neutrino-nucleon cross section [6] compared with PDF fits.

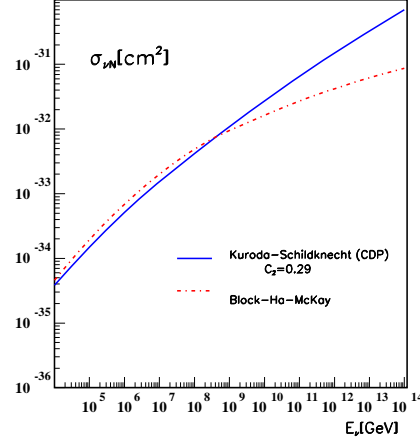


Figure 8: The neutrino-nucleon cross section and the Froissart-inspired result.

The simple explicit expression for the photoabsorption cross section, upon substitution into (6) yields the results [6] in Figure 7. The extrapolation to ultrahigh energies in the CDP agrees with results from the perturbative-QCD improved parton model. It is interesting to note that the ‘‘Froissart-inspired’’ representation [7] of the available experimental data agrees with the results from the CDP below  $E_\nu \simeq 10^{10}$  GeV, but yields a suppression of the cross section for  $E_\nu \gtrsim 10^{10}$  GeV, compare Figure 8.

## References

- [1] M. Kuroda and D. Schildknecht, Phys. Rev. **D85**, p. 094001 (2012); D. Schildknecht, Mod. Phys. Lett. **A 29**, p. 1430028 (2014); M. Kuroda and D. Schildknecht, Int. J. Mod. Phys. **A31** p. 1650157 (2016).
- [2] D. Schildknecht, *Deep inelastic scattering at low x: Generalized vector dominance and the color dipole picture*, Nucl. Phys. Proc. Suppl. **99A**, pp. 121-125; D. Schildknecht, B. Surrow and M. Tentyukov, Phys. Lett. **B 499**, pp. 116-124 (2001); G. Cvetic, D. Schildknecht, B. Surrow and M. Tentyukov, EPJ **C 20**, pp 77-91 (2001); D. Schildknecht, *Scaling in  $\gamma^*p$  total cross-sections and the generalized vector dominance/color dipole picture*, Sci. Cult. Ser.-Phys. **21**, pp. 798-803, edited by G. Bruni et al. (World Scientific, Singapore, 2002); D. Schildknecht, B. Surrow and M. Tentyukov, Mod. Phys. Lett. **A16**, pp. 1829-1840 (2001).
- [3] LHCb-CONF-2016-007, August 22, 2016.
- [4] Dieter Schildknecht, arXiv: 1611.01382
- [5] M. Kuroda and D. Schildknecht, Phys. Lett. **B638**, pp. 473-479 (2006); M. Kuroda and D. Schildknecht, EPJ **C 37**, pp. 205-222 (2004); M. Kuroda and D. Schildknecht, EPJ **C 44**, p. 613 (2005) Erratum.
- [6] M. Kuroda and D. Schildknecht, Phys. Rev. **D88**, p. 053007 (2013).
- [7] M.M. Block, P. Ha and D. McKay, Phys. Rev. **D82**, p. 077302 (2010).